https://doi.org/10.5194/acp-2020-840
Preprint. Discussion started: 31 August 2020

Atmospheric Chemistry and Physics Discussions

Stratospheric pollution from Canadian forest fires

Hugh C. Pumphrey[1], Michael J. Schwartz[2], Michelle L. Santee[2], George P. Kablick III[3], Michael D. Fromm[3], and Nathaniel J. Livesey[2]

[1]School of GeoSciences, The University of Edinburgh, Edinburgh, UK
[2]NASA Jet Propulsion Laboratory, California Institute of Technology, Pasadena, CA, USA
[3]US Naval Research Lab, Washington DC, USA

Correspondence: Hugh Pumphrey (Hugh.Pumphrey@ed.ac.uk)

Abstract. Forest fires in British Columbia in August 2017 caused a pyrocumulonimbus event that injected a polluted airmass into the lower stratosphere. The Microwave Limb Sounder (MLS) on the Aura satellite first observed the polluted airmass on 14 August 2017 and continued to observe it for 60 days (100 days in water vapour). We estimate the mass of CO injected into the stratosphere to be 2 – 3 Tg. Events such as this are rare: this is the third of four such events in the 16 years since the launch of Aura, the second-largest of the four events, and the only one in the Northern Hemisphere. Unlike the preceding two events, but like the most recent event, the polluted airmass described here had an unusually high water vapour content.

1 Introduction

The summer of 2017 saw the most destructive forest fires on record in British Columbia, Canada (Government of British Columbia, 2018). On 12 August 2017 a particularly intense cluster of fires gave rise to a strong convective event that lofted biomass-burning product gases to an altitude of 10–11 km (215 hPa). The fires are described in some detail by Peterson et al. (2018), who refer to them as the "Pacific Northwest Event"; we adopt this name and abbreviate it to PNE. The polluted airmass was transported around the world, ascending to an altitude of 20 km (46 hPa) over a period of 18 days. It remained observable for about 100 days, reaching a final altitude of 25 km (26 hPa). Lidar observations of extremely high levels of aerosol in the polluted airmass have been reported from Europe (Ansmann et al., 2018; Khaykin et al., 2018; Hu et al., 2019) and Russia (Zuev et al., 2019). Khaykin et al. (2018) also report space-based lidar data from the Cloud-Aerosol Lidar with Orthogonal Polarization (CALIOP) instrument (Winker et al., 2009), showing the global evolution of the plume.

We report here observations of some of the gas-phase components of the polluted airmass made by the Microwave Limb Sounder (MLS). The ozone and water vapour data have been reported previously (Yu et al., 2019); here we report in more detail on the full suite of biomass-burning products observed by MLS.

https://doi.org/10.5194/acp-2020-840
Preprint. Discussion started: 31 August 2020

Atmospheric Chemistry and Physics Discussions

2 Data from MLS

The MLS instrument (Waters et al., 2006) was launched in July 2004 on NASA's Aura satellite and has operated almost continuously since then. Aura is in a polar orbit with a 98° inclination angle. The MLS instrument views in the direction of travel; as a result the measurement locations lie close to the orbit track and cover the latitude range 82° S to 82° N. Once processed, the data consist of 3495 vertical profiles per day, spaced at intervals of 167 km along the orbit track. Estimated quantities include temperature, geopotential height, and the mixing ratios of 16 chemical species, including H_2O (Lambert et al., 2007), CO (Livesey et al., 2008; Pumphrey et al., 2007) and HCN (Pumphrey et al., 2018). Data are reported on pressure levels; for most products these are spaced at 6 levels per pressure decade, giving a representation with a vertical resolution of about 2.7 km. For most products the true vertical resolution is similar to this spacing, but for species with low mixing ratios and/or weak spectral lines it may be considerably poorer than this. For a few species (H_2O, O_3) the data are reported at a resolution of 12 levels per pressure decade. Full details on use of the data may be found in Livesey et al. (2018).

3 Observations

3.1 Carbon Monoxide

MLS CO data are recommended for use at pressure levels from 215 hPa ($\sim$ 11 km) up to 0.0046 hPa ($\sim$80 km). Data are reported at the 316 hPa level ($\sim$ 8 km), but these values are thought to mostly represent the real atmosphere at 215 hPa and are not recommended for any quantitative work. They can, to some extent, be a useful qualitative indicator of excess CO somewhere in the 8-10 km altitude range; we show the 316 hPa data in some of the figures in this paper, but do not use them to derive any quantitative results.

Enhanced values of CO from the Pacific Northwest Event were first observed on 14 August 2017. Figure 1 shows MLS CO over North America at this time, at 215 hPa. The maximum values seen here are about 1.2 ppmv; this is about 24 times the typical zonal mean value of 50 ppbv and about 6 to 8 times the typical daily maximum value. Figure 2 shows a time series of the maximum CO values observed at several pressure levels. It is clear that the polluted airmass reached 215 hPa almost immediately. From there, it ascended fairly rapidly to 100 hPa and then more slowly from 100 hPa to 46 hPa.

To summarise the whole event, we applied the strategy used by Pumphrey et al. (2011) to detect values that exceed the usual spread expected for a given latitude band. We found the mean value and standard deviation for all measurements in a given latitude band and at a given pressure level. We then describe the CO at a point as "enhanced" if its mixing ratio was more than a chosen number, α, of standard deviations above the mean. The value chosen for α is somewhat arbitrary and was different for each level: $\alpha = 5.7$ at 215 hPa, $\alpha = 4.6$ at 147 and 100 hPa and $\alpha = 3.9$ at all other pressure levels. These choices are made in order to show the interesting events while rejecting almost all of the background points. An iterative approach is used to ensure that the mean and standard deviation are calculated from the unaffected points; there are few enough affected points that this calculation converges very quickly.

https://doi.org/10.5194/acp-2020-840
Preprint. Discussion started: 31 August 2020

Atmospheric Chemistry and Physics Discussions

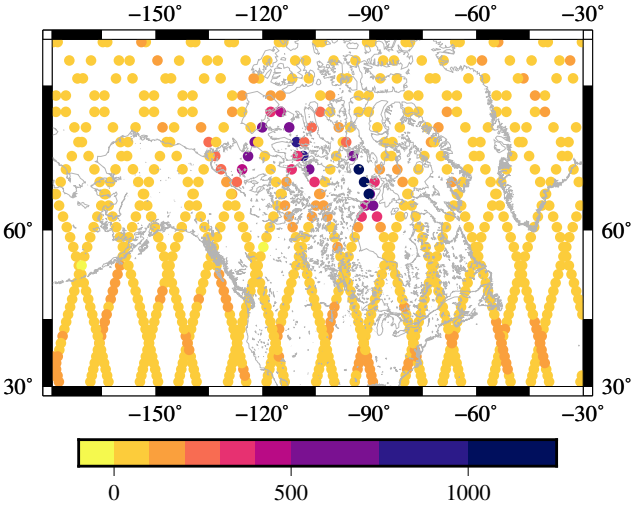

Figure 1. MLS measurements of CO (in ppbv) at 215 hPa (≈ 11 km altitude) on 14-15 August 2017. These are the first two days after the PNE on which MLS observed the enhanced CO values.

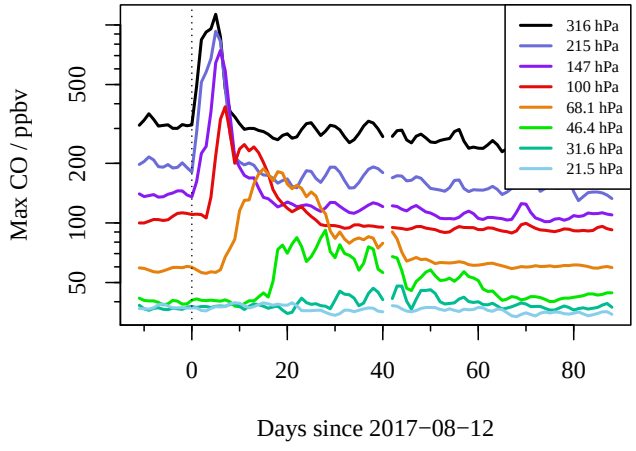

Figure 2. Time series of maximum CO values observed polewards of 25° N. The values shown are averages of the ten highest observed values on each day between 15° N and 83° N. A 3-day smoothing has been applied to each curve.

Figure 3 shows the locations where enhanced CO was detected. The plume is first observed over northwestern Canada, travelling southeastwards and then eastwards across northern Canada and then across the Atlantic to Europe. The behaviour of the plume while over Eurasia is more complex. After 30 days, one part of it reaches northwestern China, where it divides into two parts, one heading east across the Pacific at about 47° N and the other returning westwards across the Atlantic at about 33° N.

As the polluted airmass moves far more rapidly in the zonal than the meridional direction, it is helpful to plot it against time and longitude, as in Fig. 4. The ascent of the polluted airmass (shown by the changing colour and shape of the points) is

https://doi.org/10.5194/acp-2020-840
Preprint. Discussion started: 31 August 2020

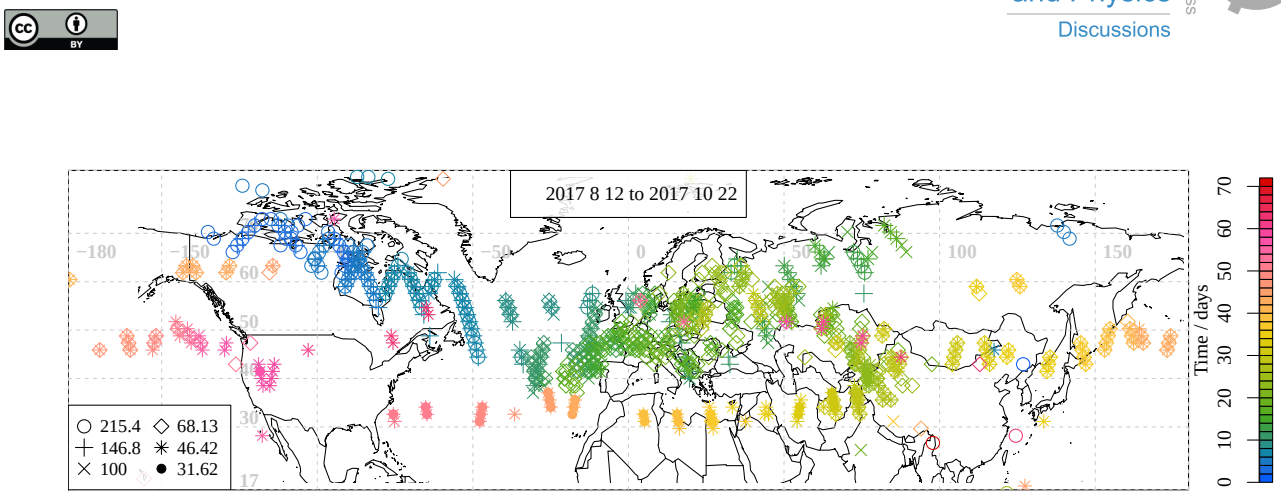

Figure 3. Map showing the locations of MLS observations of enhanced CO (defined as described in the text). Colours show time in days after 12 August 2017. Symbols show pressure level in hPa.

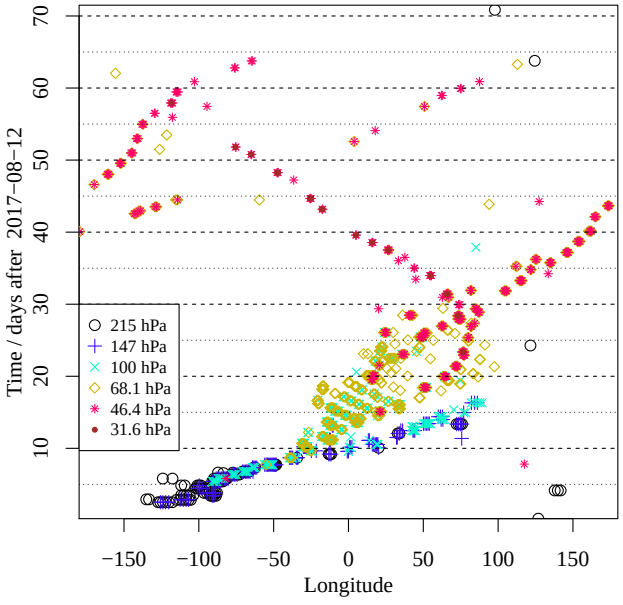

Figure 4. Longitudes of enhanced CO (as defined in the text), plotted as a function of time. Colours and symbols represent pressure.

clearly visible in this figure. It can also be seen in Fig. 4 that the polluted airmass is divided into two parts on three occasions: at approximately 9 days, 16 days and 41 days after 12 August 2017. After the first division, one branch remains at 147 to 100 hPa, travels more rapidly than the other branch and is last seen on day 16 near 80° E, 70° N. The higher branch is at 100 to 68 hPa at day 9 and continues to ascend. It appears to divide into two parts somewhere around day 16; these two parts appear in Fig. 4 to cross over at around day 30, after which one part travels east and one west. The more northern part travels eastward from northern China across the Pacific Ocean, while the more southern part rises to 31.6 hPa and moves westward across northern Africa and the Atlantic Ocean. Around day 41, the eastward-travelling part appears to divide into further parts. The faster-travelling part is last seen on day 60 at 90° E; the slower part is last seen on day 63 at 60° W.

https://doi.org/10.5194/acp-2020-840
Preprint. Discussion started: 31 August 2020

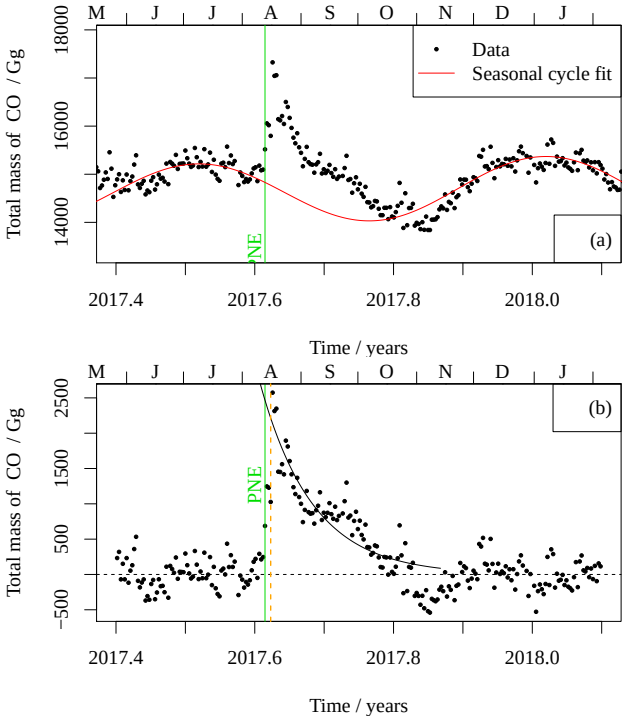

Figure 5. (a) Total mass of CO observed by MLS poleward of 27.5° N and at altitudes between 215 hPa and 31 hPa. (b) As (a), but with the seasonal fit subtracted from the data, and an exponential fitted to the measurements made after the fire. The vertical dashed orange line marks 16 August 2017: the time of the earliest data used in the exponential fit.

We can obtain an estimate of the total injected mass of CO by integrating the MLS data into partial column (215 hPa to 31 hPa) values and summing over all latitudes affected by the event. The seasonal behaviour of CO is fitted with a mean value and annual and semiannual sinusoids as shown in Fig. 5(a); this fit ignores the data for a period of 99 days after the PNE. Subtracting this first fit from the data leaves a fairly featureless time series apart from a sudden increase after the fire and a decay after that; we fit the decay with an exponential:

$$M = M_0 \exp\left(-\frac{t}{t_d}\right)$$

The exponential curve is shown in Fig. 5(b). The injected mass, M_0, is 2500 ± 150 Gg, with a decay time t_d of 27 ± 2 days; the errors here are those given by the `nlm()` function in R (R Core Team, 2018). The CO data from the first three days after the event are not well fitted by the exponential used to fit the subsequent days, presumably because the plume has a small horizontal extent and lies in between the MLS orbit tracks. These days are therefore excluded from the exponential fit. The values of M_0 and t_d obtained depend rather critically on exactly which of these early points are included. The given values are obtained using data from 16 August 2017 onward; this date is marked on Fig. 5 (b) with a dashed line. This date was chosen because to use a later date is to throw away data that are part of the exponential decay, while to use earlier dates is to include data that

https://doi.org/10.5194/acp-2020-840
Preprint. Discussion started: 31 August 2020

Atmospheric Chemistry and Physics Discussions

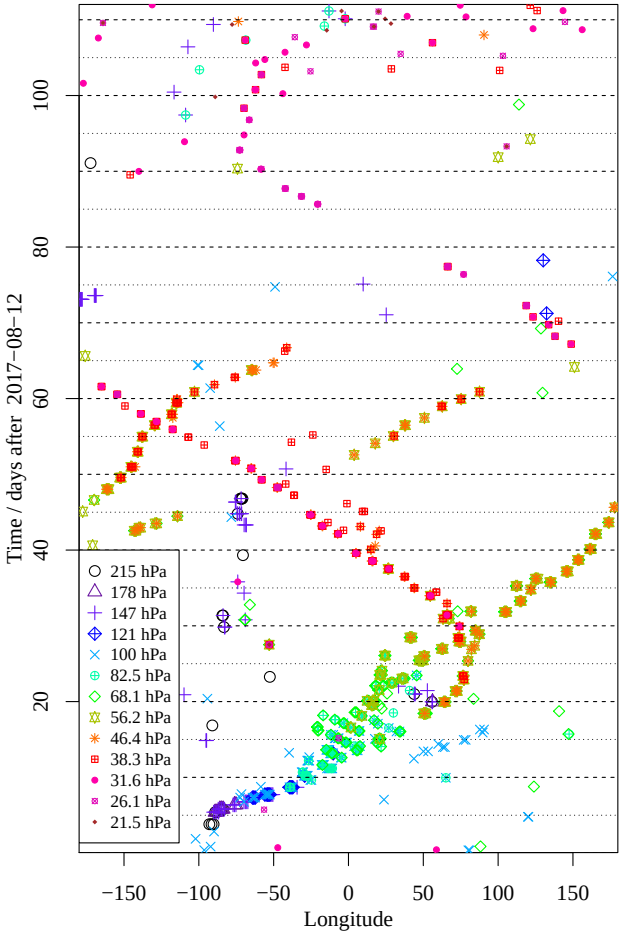

Figure 6. Longitudes of enhanced H_2O, plotted as a function of time. Colours and symbols represent pressure.

are not part of the exponential decay. A cutoff date earlier than 16 August 2017 results in smaller estimates of M_0 and larger estimates of t_d; later dates give a range of similar values with larger errors. The values obtained are also sensitive to the end of the window used for the exponential fit. A more conservative estimate of the parameters and their errors, taking into account the spread of values obtained with reasonable ranges of start and end dates, is $M_0 = 2400 \pm 300$ Gg and $t_d = 28 \pm 10$ days.

3.2 Water vapour

The event described in this paper differs from the Black Saturday event (Pumphrey et al., 2011) in that a large amount of water vapour is found in the polluted airmass. Figure 6 shows the longitudes of unusually high water vapour in the same manner as Fig. 4. The values chosen for the parameter α, described above for CO, vary from $\alpha = 6$ at 147 hPa to $\alpha = 2$ between 38 and 21 hPa. Many points with enhanced water vapour are found between 215 and 147 hPa and between 60° E and 180° E. These points are clearly not connected with the PNE so we have removed them from Fig. 6. It is clear from a comparison between

https://doi.org/10.5194/acp-2020-840
Preprint. Discussion started: 31 August 2020

Atmospheric Chemistry and Physics Discussions

Table 1. Summary of species observed by MLS to have clearly enhanced mixing ratios in the polluted airmass. The first and last days after 12 August 2017 are listed as d_0 and d_1; the highest and lowest pressures at which unusual values are observed are listed as p_0 and p_1. The BB? column indicates whether or not the species is a genuine biomass burning product. For some species the enhanced values are thought to be caused by a measurement problem (see main text). Species observed by the instrument but with no unusual values detected in the polluted airmass are: O_3, SO_2, BrO, HNO_3, N_2O.

Species	d_0	d_1	p_0	p_1	BB?
CO	2	63	316	31	yes
H_2O	2	90	316	26	yes
HCN	8	59	100	31	yes
CH_3CN	5	58	147	31	yes
CH_3Cl	5	26	147	68	yes
CH_3OH	5	16	147	68	yes
ClO (640 GHz)	5	33	147	46	no
HO_2	5	11	147	68	no
HOCl	5	8	147	100	no
HCl	5	7	147	100	no

Figs. 4 and 6 that, where both species are enhanced, the enhanced CO and H_2O occur in the same locations. The enhanced CO can be detected against the background variability by the method described 2–3 days before the enhanced H_2O becomes apparent. Inspection of daily maps of the data reveals that H_2O is clearly enhanced on 14 August 2017 between 60°N and 70°N. The algorithm used fails to detect the enhancement at this time because of the very large background variability at lower latitudes.

After about 50 days the water vapour in the polluted airmass exceeds the background value to a greater extent than is the case for CO. After 63 days, the polluted airmass can only be identified in the water vapour data; this is presumably due to the short chemical lifetime of CO in the stratosphere. A small parcel of enhanced H_2O may be seen travelling westwards from 150° E to 80° W, between 65 and 90 days after the event, before ceasing to travel westwards, and fading into the background.

3.3 Other species

All chemical species observed by MLS were examined for the few months after the PNE using the same thresholding technique as for CO and H_2O. For ClO, we examined the standard (640 GHz) product, a secondary product derived from the 190 GHz measurements, and a product derived from the 640 GHz data while also estimating CH_3OH. The species fall into three categories:

- Species for which no anomalous mixing ratios in the plume rise above the background variability: O_3, SO_2, BrO, HNO_3, N_2O, ClO (190 GHz). Some of these species (O_3 and N_2O are the most obvious) nevertheless show some correlation with CO values in the plume as we show later.

https://doi.org/10.5194/acp-2020-840
Preprint. Discussion started: 31 August 2020


Atmospheric Chemistry and Physics Discussions

– Genuine biomass burning products: CO, H_2O, HCN, CH_3CN, CH_3OH and CH_3Cl; elevated values of these are observed for about 60 days (100 days for H_2O).

– Species for which anomalous measurements are believed to be artifacts arising from spectral interference due to the presence of another molecule: HOCl, HO_2, HCl, ClO (640 GHz).

A summary of the ranges of time and altitude over which each species has unusual values is shown in Table 1. Pumphrey et al. (2011) demonstrate that an airmass containing biomass-burning products may appear from the MLS level 2 data to contain enhanced amounts of the 640 GHz ClO product, but that this is actually caused by enhanced amounts of methanol (CH_3OH), which has a similar spectral signature to ClO in the passband of the MLS 640 GHz radiometer.

As is the case for many MLS data products, CH_3OH is produced from a dedicated retrieval "phase", in which a ClO product (not the standard one) is also retrieved (see Livesey et al. (2018) for details). The ClO data from the methanol phase show far less correlation with CO than the standard 640 GHz ClO product. This also suggests that the enhanced values seen in the standard 640 GHz ClO product are an artefact caused by enhanced methanol. HOCl, HO_2 and CH_3Cl are all detected via spectral lines that are very close to the CH_3OH lines. It seems reasonable to suppose that HOCl and HO_2 appear to be enhanced in the MLS data due to spectral contamination from CH_3OH, especially as they are both observed only for a very short period. CH_3Cl, on the other hand, is known to be a biomass-burning product (Santee et al. (2013) and references therein); its spectral signature is sufficiently different from that of ClO (or CH_3OH) that the enhancement observed is almost certainly genuine. HCl, which shows the smallest enhancement in the plume, is observed at a different frequency from the ClO, CH_3OH and CH_3Cl lines, but one very close to the main CH_3CN lines in the MLS 640 GHz radiometer. Although HCl is a minor fire product (mainly produced from the burning of garbage (Akagi et al., 2011)), it seems likely that the enhanced values observed are spurious and are caused by the large amounts of CH_3CN in the plume.

The relationships between species in the plume were investigated further by calculating a linear fit between enhanced CO and a given species at the same retrieval level and location. Data from profiles immediately adjacent to the plume are included to provide an appropriate baseline. We show an example in Fig. 7 in which the other species is CH_3CN. Plotting the data in this manner reveals that in some cases (O_3, N_2O) there is a correlation between the two species, even when the non-CO species does not have values outside its usual range. For other species (SO_2, HNO_3, BrO), no such correlation is observed, or the correlation is small enough to suggest that it is an instrumental rather than a geophysical effect. We note values of the linear fit slope in Table 2 and show a selection of the data from Table 2 in Fig. 8. For some species (including the CH_3CN shown in Fig. 7) we have used data outside the vertical range recommended by the MLS team. This was done where the correlation with CO was clear; we note that the linear fit slopes will not be affected by a constant bias in the mixing ratio of either CO or the other species. For species produced by biomass burning and which have similar lifetimes to CO in the lower stratosphere, we would expect the ratios observed in Table 2 to be constant with altitude and to be in reasonable agreement with the emission ratios measured previously. The relationships with CO of CH_3CN and CH_3Cl show relatively little variation with height. The slopes we obtain are generally within the published range; for CH_3Cl this range is rather large. The methanol/CO ratio is within the rather wide range of published values and decreases with height. This might appear to suggest that methanol undergoes

https://doi.org/10.5194/acp-2020-840
Preprint. Discussion started: 31 August 2020

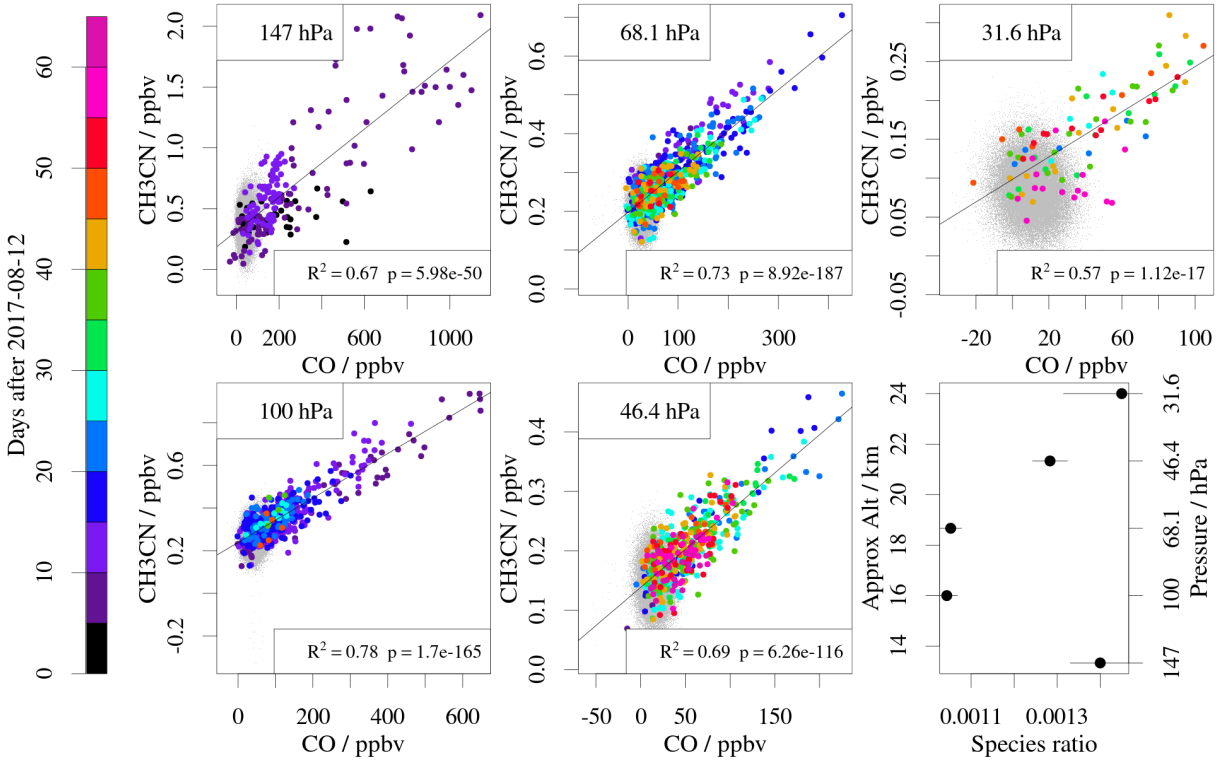

Figure 7. Scatter plots of the mixing ratio of CH_3CN against that of CO at five pressure levels between 14 August 2017 and 30 October 2017. Only data from north of 27.5° N are shown. The small grey dots show the entire dataset within the stated latitude and time ranges. The large coloured dots are points with enhanced CO and points within 350 km (48 s) of those points along the orbit track. The linear fits use the large points only and are performed using the `lm()` function of R (R Core Team, 2018); the R^2 and p-value are shown for each fit. The lower right panel shows the slopes of the linear fits as a function of altitude.

chemical loss in the plume more rapidly than CO, but the MLS methanol data are potentially useful only at 147 hPa (and at low latitudes at 100 hPa), so any such conclusion must be regarded as speculative. The agreement between our value at 147 hPa and the published values is reasonable given the large variability in the latter.

The H_2O/CO ratio varies considerably with height between 215 and 68 hPa, but is approximately constant between 68 and 31 hPa. The standard 640 GHz ClO data behave in a similar manner to the biomass-burning products. This is compatible with the fact that the standard ClO retrieval may have been affected by interference or contamination from methanol (Pumphrey et al., 2011); as noted above, the other ClO products are not enhanced so the elevated abundances of the standard product are probably due to high values of methanol.

Yu et al. (2019) showed that the negative anomaly in ozone and the positive anomaly in H_2O observed by MLS were a consequence of the transport of tropospheric air into the stratosphere (and not in situ chemical loss in the case of ozone). Such upward transport probably also gave rise to increases in N_2O and thus positive correlations between N_2O and CO. Kablick

https://doi.org/10.5194/acp-2020-840
Preprint. Discussion started: 31 August 2020

Atmospheric Chemistry and Physics Discussions

Table 2. Ratios between the mixing ratio of various species and that of CO, at various pressure levels. Subscripts indicate error in the last digit. The errors are those returned by a standard fitting program (the `lm()` function in R). The right-hand column shows values from the literature converted into ratios with CO. Superscripts in this column indicate sources: Randerson et al. (2017)[1], Rinsland et al. (2007)[2], Simpson et al. (2011)[3], Akagi et al. (2011)[4]. Published values shown are all for boreal forests with the exception of HCl. A "—" indicates either that the species does not have good data at that level or that the linear fit is not significant at the 99% level ($p > 0.01$).

Species	215 hPa	147 hPa	100 hPa	68 hPa	46 hPa	31 hPa	Other measurements
H_2O	119_5	47_2	18.5_8	32.2_7	39_1	35_4	—
HCN	—	—	—	0.00097_4	0.00167_4	0.0022_2	$0.012^{1,4}$, 0.00242^{2}_{32}, 0.0082^{3}_{20}
CH_3CN	—	0.00140_7	0.00104_3	0.00105_3	0.00128_4	0.00145_{14}	0.0032^{4}, 0.0018^{3}_{3}
CH_3Cl	—	0.00109_7	0.00141_5	0.00127_7	0.0012_1	0.0011_4	0.0056^{2}, 0.00014^{3}_{3}
ClO std	—	0.0048_2	0.0056_2	0.0044_1	0.0036_2	0.0014_5	—
HCl std	—	0.0039_2	0.0018_1	-0.0010_2	-0.0033_4	—	0.0010^{4}_{10} (chaparral)
CH_3OH	—	0.012_1	0.0107_5	0.0058_2	0.0062_4	0.0024_9	$0.019^{1,4}_{13}$, 0.00015^{3}_{15}
O_3	-0.15_2	-0.23_3	-0.39_8	-1.81_{15}	-5.2_3	-6_1	—
N_2O	—	—	—	0.21_1	0.32_3	0.4_1	0.0020^{1}

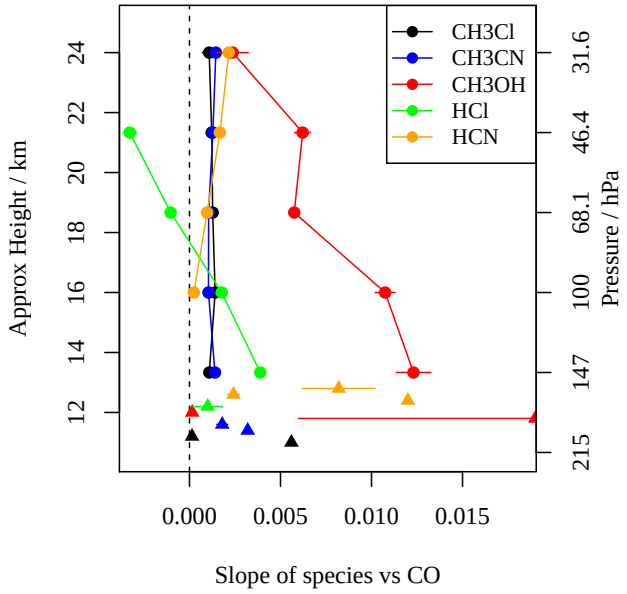

Figure 8. Slopes of scatter plots of various species against CO; the slopes are calculated as in the example shown in Fig. 7. Triangles are the data from the "other measurements" column of Table 2, with their error bars (where available). All the triangles refer to measurements made in the troposphere; their position in the vertical has no meaning.

https://doi.org/10.5194/acp-2020-840
Preprint. Discussion started: 31 August 2020

Atmospheric Chemistry and Physics Discussions

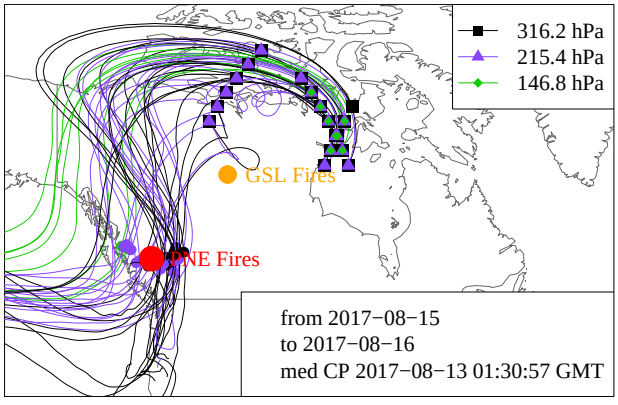

Figure 9. Back trajectories launched at points where MLS observed large values of CO. The location of the Pacific Northwest Event (PNE) is marked in red. Where the trajectories pass within 400 km of the PNE, the closest point is marked with a dot.

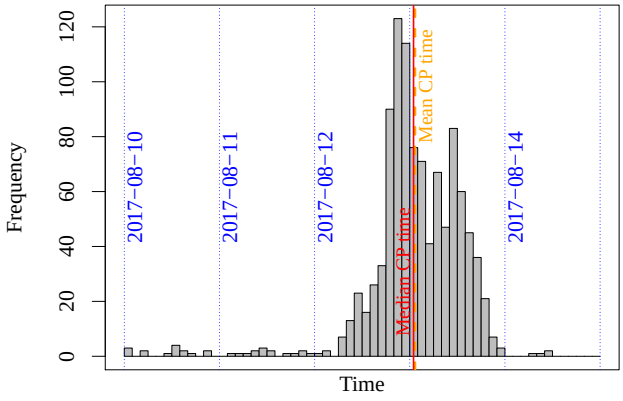

Figure 10. Histogram of closest-pass times of trajectories to the PNE. The median and mean values are marked in red and orange respectively. The dotted blue lines are at 00:00 UTC.

et al. (2020) discuss the low ozone and high N_2O values associated with the Australian New Year (ANY) fires of December 2019. They attribute these anomalies to rapid ascent of tropospheric air; it appears likely that the ozone and N_2O in the PNE behaved in a similar way.

4 Trajectory and dispersion modelling

4.1 Back Trajectories

Back trajectories from the MLS observations in the first few days after the event were calculated using the FLEXTRA trajectory model (Stohl et al., 1995), driven by analyses from the National Centers for Environmental Prediction (NCEP) Global Forecast System (GFS) analyses (National Centers for Environmental Prediction, 2000). Trajectories launched at 316 and 215 hPa pass

https://doi.org/10.5194/acp-2020-840
Preprint. Discussion started: 31 August 2020

Atmospheric Chemistry and Physics Discussions

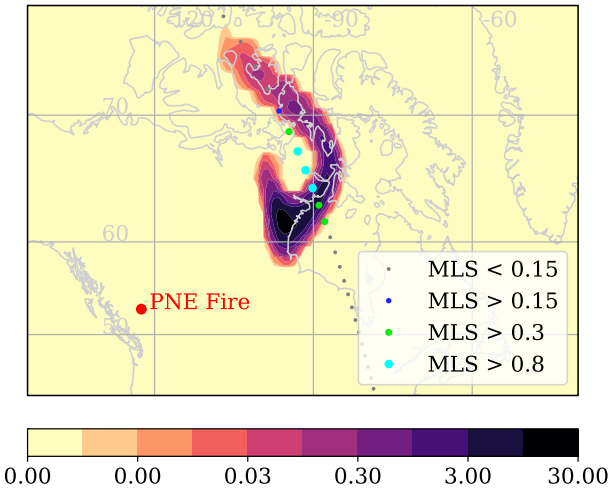

Figure 11. FLEXPART CO mixing ratio in ppmv at altitude 12 km on 15 August 2017 at 18:00, with MLS CO mixing ratio (also in ppmv) from an orbit at a matching time.

reasonably close to the Pacific Northwest Event; we show examples in Fig. 9. Although MLS observes enhanced CO at the 147 hPa level at this time, trajectories launched at this level pass far to the west of the PNE. This suggests that over these first few days the polluted airmass is closer to 215 hPa than to 147 hPa. There were other forest fires burning at the same time as the PNE, notably in the region around Lake Athabasca and the Great Slave Lake (GSL); the location of these fires is marked on Fig. 9. The trajectories make it reasonably clear that the source of the polluted airmass observed by MLS is the Pacific Northwest Event and not the fires near the Great Slave Lake.

By launching trajectories at many points spread between the MLS observations of high CO, both vertically and along the measurement track, we obtain sufficient times of closest pass to the PNE to construct a histogram, as shown in Fig. 10. The mean and median closest pass times are 01:20 UTC and 00:57 UTC respectively on 2018-08-13. The standard deviation of the closest-pass times is 12 hours. The closest pass times are in good agreement (given their own standard deviation) with the times reported by Peterson et al. (2018), who state that pyrocumulonimbus clouds (pyroCb) are observed to develop between 23:00 UTC on 12 August 2017 and 00:30 UTC on 13 August 2017, and that they remain active for 1–4 hours.

4.2 Plume trajectory modelling

The FLEXPART model (Stohl et al., 2005) was used to model the dispersion of the plume from the Pacific Northwest Event. FLEXPART allows the user to release a mass of a pollutant at a chosen place and time and to observe how it disperses. We released the pollutant in a small cuboid region; the release is defined by the location and size of this region, by a start and end time, and by the mass released. We show in Fig. 11 an example of FLEXPART output for a time approximately 66 hours after the PNE. An MLS orbit that passes through the polluted airmass at that time is also shown; points where the MLS CO is enhanced are marked and lie close to the modelled plume.

https://doi.org/10.5194/acp-2020-840
Preprint. Discussion started: 31 August 2020

Atmospheric Chemistry and Physics Discussions

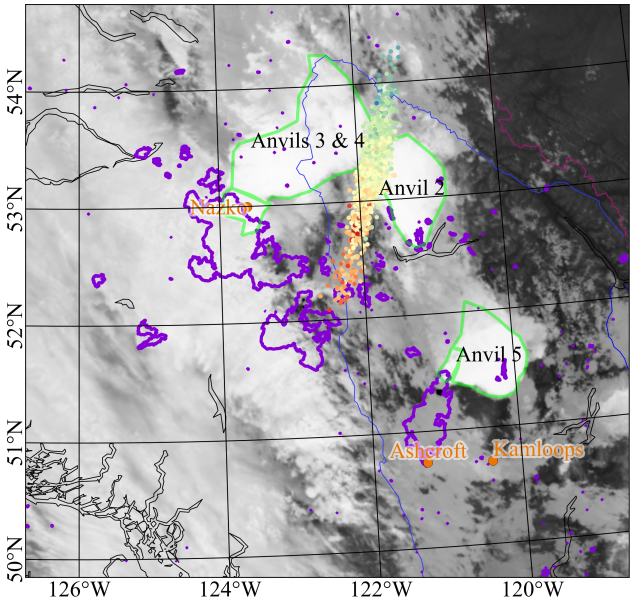

Figure 12. Map of the source region, showing areas burned in 2017 (purple; some areas are sufficiently small that the contours enclosing them appear as dots) and anvils observed in AVHRR data (green). The anvils are numbered using the same scheme as Peterson et al. (2018); their anvil 1 is outside the area shown here. The greyscale backdrop is the AVHRR channel 5 (thermal IR) image taken at about 02:00 GMT. The small points are the MCMC solutions for the apparent origin of the polluted airmass and are coloured according to time; see text for details.

We adjust the properties of the mass released to best match the MLS observations using the Markov Chain Monte Carlo (MCMC) inverse modelling technique (van Ravenzwaaij et al., 2018). As FLEXPART is not able to model the self-lofting of the polluted airmass, we used only the first few days of data after the fire. Some experimentation demonstrated that the data do not provide sufficient information to determine the horizontal extent of the release region, nor its extent in time. We therefore constrained the region to be 0.5° wide in longitude, 0.375° wide in latitude and 1.5 hours in duration. (These choices were somewhat arbitrary and were intended to ensure that the box was smaller than the observed pyroCb clouds.) The estimated quantities were then the location and time of the release cuboid, its vertical extent, and the total mass of CO released.

We show the horizontal release locations found by the MCMC approach in Fig. 12. There were several large anvil clouds in the area at the time; these are clearly visible in AVHRR images and are outlined in green in Fig. 12. The MCMC solutions have a standard deviation of about 6 km perpendicular to the wind direction and 30 km in the wind direction. The injection altitude is determined rather precisely: 11.5 ± 0.1 km; as expected from the back trajectories, this is closer to 215 hPa than to 147 hPa. The injected mass is 620 ± 80 Gg, considerably smaller than the value of 2400 ± 300 Gg that we obtained by the simple method discussed in section 3.1. This is qualitatively reasonable, given that the MCMC approach only considers CO that is observable by MLS near the start of the event, while the simple method of section 3.1 includes CO that was injected at too low an altitude for MLS to observe it and subsequently ascended to observable altitudes. release time is about 5:00 UTC on

https://doi.org/10.5194/acp-2020-840
Preprint. Discussion started: 31 August 2020


Atmospheric Chemistry and Physics Discussions

13 August 2017, with a spread of possible values between 3:30 UTC and 7:30 UTC. This is later than the time estimated using FLEXTRA trajectories, but is well within the 12 hour standard deviation of the FLEXTRA results. As noted above, Peterson et al. (2018) report the pyroCb events as beginning between 12 August 2017, 23:00 and 13 August 2017, 00:30 and lasting 1-4 hours. The release times we determined using FLEXPART and the MLS data are at the late end of this range.

5 Discussion

Significant injections of pyroconvective plumes into the stratosphere generally require both extremely intense fires and particular meteorological conditions, such as those preceding the passage of a cold front. The meteorology surrounding the Pacific Northwest Event is described in some detail by Peterson et al. (2018); the fire indeed occurred while a cold front was approaching.

Most forest fires do not produce a pyroCb cloud. Moreover, most pyroCb clouds do not extend to a great enough altitude to loft the products high enough for MLS to observe them. The only events in the MLS record that are in any way comparable to the PNE are the Black Saturday fire, which occurred in Australia in February 2009 (Pumphrey et al., 2011), and the Australian fires of December 2019 to January 2020 (paper in preparation, also Kablick et al. (2020), who refer to this as the Australian New Year (ANY) event). The mass of CO injected into the lower stratosphere by the Black Saturday fire was, when estimated by the technique of section 3.1, 1.3 Tg — just over half of the mass injected by the PNE. Like the PNE, the Black Saturday fire occurred at a time when a cold front was approaching (Dowdy et al., 2017). The 2019/20 ANY fire injected a mass of CO considerably larger even than the PNE: initial esimates, again using the method of section 3.1, place this mass in the range 8–10 Tg. MLS also observed enhanced CO from the Great Divide fires in Australia in December 2006. These fires burned for two months, but MLS only observed enhanced CO from them for a short time, beginning on 2006-12-12. The injected mass of CO from the Great Divide fires was between 1.5 and 1.8 Tg, similar to that from the PNE, but the polluted airmass did not ascend in the manner observed with the PNE, ANY and Black Saturday events, and was observed by MLS for only 10 days (Pumphrey et al., 2011).

The MLS data shown in this paper are for most species the first data reported from the PNE. Measurements of aerosols emitted by the event have been reported in some detail. Zuev et al. (2019), Hu et al. (2019), Ansmann et al. (2018) and Khaykin et al. (2018) report ground-based lidar observations of the PNE plume as it passed over Europe. Khaykin et al. (2018) also report aerosol data from the CALIOP lidar instrument on the CALIPSO satellite. The maps of the CALIOP data are similar to Fig. 3, indicating that the aerosol and CO travelled together; presumably the aerosol particles were too small to settle out on the timescale over which the CO was observed. Khaykin et al. (2018) suggest that the pollution is from fires near Lake Athabasca; we show clearly that it is from British Columbia and from the vicinity of the Pacific Northwest Event as described by Peterson et al. (2018). Ansmann et al. (2018) ascribe the source of the pollution to British Columbia in agreement with our conclusions. In addition to the MCMC results, Fig. 12 shows the areas burned in 2017 marked in purple (British Columbia Wildfire Service, 2018). Figure 12 also shows the AVHRR thermal image; three large anvils of high cloud are clearly visible. Examination of the visible bands of the same image suggests that the anvils marked “Anvil 3 & 4” and “Anvil 5” have an active

https://doi.org/10.5194/acp-2020-840
Preprint. Discussion started: 31 August 2020


Atmospheric Chemistry and Physics Discussions

pyroCb cloud at the southwest edge. It is not clear from the visible images that an active pyroCb is associated with Anvil 2; images taken during the previous two hours (Peterson et al., 2018) show that Anvil 2 formed near 00:00 UTC. Anvil 3 also formed around 00:00 UTC; Anvil 4 formed half an hour later and had merged with Anvil 3 by 01:45 UTC.

The possible solutions for the source of the polluted airmass that emerge from the MCMC inverse method are shown in Fig. 12 as a cloud of small points. The colours of these dots indicate the time, varying from 2:00 GMT (red) to 5:00 GMT (blue). The location of these dots suggests that the polluted airmass observed by MLS is probably associated with Anvils 2, 3 and 4 and is less likely to be associated with Anvil 5. This in turn suggests that the emissions come from the plateau complex of fires (west of Nazko) and not from the Elephant Hill fires (north of Ashcroft).

The polluted airmasses from the PNE and ANY contained large amounts of water — this distinguishes them from the Black Saturday event, in which the water content of the polluted airmass was similar to that of the surrounding air, except at 100 hPa and lower altitudes during the first few days of the event.

The rapid ascent of the polluted airmass from the PNE is due to its containing a large amount of black carbon aerosol (Yu et al., 2019; Kablick et al., 2020). The aerosol absorbs incident sunlight, heating the polluted airmass and causing it to rise. The event can in some ways be considered a small-scale demonstration of what would happen in the aftermath of a nuclear war: such a war would cause widespread fires that would put a great deal more black carbon into the middle atmosphere than the PNE did. Self-lofting of this carbon (as demonstrated by the PNE) would raise it to an altitude where it would remain for a number of years, giving rise to the so-called *nuclear winter* [Robock et al. (2007) and references therein]. Simulations (Reisner et al., 2018; Robock et al., 2007) of the response of the climate to a regional-scale nuclear war disagree on the severity of this effect. However, much of the disagreement is caused by widely different estimates of how much black carbon would reach the stratosphere from a given nuclear explosion. Once it did reach the stratosphere, the black carbon aerosol from a nuclear war would ascend in the manner we observe in the PNE.

6 Conclusions

The Pacific Northwest Event was a forest fire accompanied by unusually strong convection, injecting both aerosol and gas-phase pollutants into the stratosphere. Observations of gas-phase pollutants from the MLS instrument show that the polluted airmass reached all longitudes on a timescale of 60 days and ascended to an altitude of 24 km. The polluted airmass was much wetter than the surrounding air in the stratosphere; in this respect it was different from the otherwise similar Black Saturday event and similar to the recent ANY event. The polluted airmass contained biomass-burning products HCN, CH_3CN, CH_3Cl and CH_3OH in broadly similar proportions to CO as observed by other techniques in other biomass-burning events.

Events of the type we describe here are rare; the PNE, ANY, Black Saturday and Great Divide fires are the only such events in the MLS dataset at the time of writing. Whether they will become rarer or more frequent as the climate changes over the coming decades remains to be seen.

https://doi.org/10.5194/acp-2020-840
Preprint. Discussion started: 31 August 2020

Atmospheric Chemistry and Physics Discussions

Code and data availability. The FLEXTRA and FLEXPART models are available at https://www.flexpart.eu/. The MLS data used in this paper are available at https://disc.gsfc.nasa.gov/. The data for each species has a separate DOI, e.g. 10.5067/Aura/MLS/DATA2005 (CO), 10.5067/Aura/MLS/DATA2009 (H2O). The AVHRR L1B data can be obtained from https://www.bou.class.noaa.gov/saa/products/welcome

Author contributions. HCP wrote most of the paper. MJS provided some of the data analysis and suggested the use of figures 4, 6 and 7. MLS provided advice on the CH_3OH, ClO, CH_3CN and CH_3Cl products. MLS, MJS, GPK, MDF and NJL suggested many improvements to the text.

Acknowledgements. Work at the Jet Propulsion Laboratory, California Institute of Technology, was done under contract with the National Aeronautics and Space Administration. MLS research at Edinburgh was funded by NERC under grant NE/E003990/1 and previous grants.

https://doi.org/10.5194/acp-2020-840
Preprint. Discussion started: 31 August 2020

Atmospheric Chemistry and Physics Discussions

References

Akagi, S. K., Yokelson, R. J., Wiedinmyer, C., Alvarado, M. J., Reid, J. S., Karl, T., Crounse, J. D., and Wennberg, P. O.: Emission factors for open and domestic biomass burning for use in atmospheric models, Atmospheric Chemistry and Physics, 11, 4039–4072, https://doi.org/10.5194/acp-11-4039-2011, https://www.atmos-chem-phys.net/11/4039/2011/, 2011.

Ansmann, A., Baars, H., Chudnovsky, A., Mattis, I., Veselovskii, I., Haarig, M., Seifert, P., Engelmann, R., and Wandinger, U.: Extreme levels of Canadian wildfire smoke in the stratosphere over central Europe on 21–22 August 2017, Atmospheric Chemistry and Physics, 18, 11 831–11 845, https://doi.org/10.5194/acp-18-11831-2018, https://www.atmos-chem-phys.net/18/11831/2018/, 2018.

British Columbia Wildfire Service: Fire Perimeters — Historical, https://catalogue.data.gov.bc.ca/dataset/22c7cb44-1463-48f7-8e47-88857f207702, accessed: 2019-06-29, 2018.

Dowdy, A. J., Fromm, M. D., and McCarthy, N.: Pyrocumulonimbus lightning and fire ignition on Black Saturday in southeast Australia, J. Geophys. Res. Atmos., 122, 7342–7354, https://doi.org/10.1002/2017JD026577, 2017.

Government of British Columbia: 2017 Wildfire Season Summary, https://www2.gov.bc.ca/gov/content/safety/wildfire-status/about-bcws/wildfire-history/wildfire-season-summary, accessed: 2017-06-17, 2018.

Hu, Q., Goloub, P., Veselovskii, I., Bravo-Aranda, J.-A., Popovici, I. E., Podvin, T., Haeffelin, M., Lopatin, A., Dubovik, O., Pietras, C., Huang, X., Torres, B., and Chen, C.: Long-range-transported Canadian smoke plumes in the lower stratosphere over northern France, Atmospheric Chemistry and Physics, 19, 1173–1193, https://doi.org/10.5194/acp-19-1173-2019, https://www.atmos-chem-phys.net/19/1173/2019/, 2019.

Kablick, III, G. P., Allen, D. R., Fromm, M. D., and Nedoluha, G. E.: Australian pyroCb smoke generates synoptic-scale stratospheric anticyclones, Geophysical Research Letters, 47, e2020GL088 101, https://doi.org/10.1029/2020GL088101, 2020.

Khaykin, S. M., Godin-Beekmann, S., Hauchecorne, A., Pelon, J., Ravetta, F., and Keckhut, P.: Stratospheric smoke with unprecedentedly high backscatter observed by lidars above southern France., Geophys. Res. Lett., 45, 1639–1646, https://doi.org/10.1002/2017GL076763, 2018.

Lambert, A., Read, W., Livesey, N., Santee, M., Manney, G., Froidevaux, L., Wu, D., Schwartz, M., Pumphrey, H., Jimenez, C., Nedoluha, G., Cofield, R., Cuddy, D., Daffer, W., Drouin, B., Fuller, R., Jarnot, R., Knosp, B., Pickett, H., Perun, V., Snyder, W., Stek, P., Thurstans, R., Wagner, P., Waters, J., Jucks, K., Toon, G., Stachnik, R., Bernath, P., Boone, C., Walker, K., Urban, J., Murtagh, D., Elkins, J., and Atlas, E.: Validation of the Aura Microwave Limb Sounder middle atmosphere water vapor and nitrous oxide measurements, J. Geophys. Res, 112, D24S35, https://doi.org/10.1029/2007JD008752, 2007.

Livesey, N. J., Filipiak, M., Froidevaux, L., Read, W., Lambert, A., Santee, M., Jiang, J., Pumphrey, H., Waters, J., Cofield, R., Cuddy, D., Daffer, W., Drouin, B., Fuller, R., Jarnot, R., Jiang, Y., Knosp, B., Li, Q., Perun, V., Schwartz, M., Snyder, W., Stek, P., Thurstans, R., Wagner, P., Avery, M., Browell, E., Cammas, J.-P., Christensen, L., Diskin, G., Gao, R.-S., Jost, H.-J., Loewenstein, M., Lopez, J., Nedelec, P., Osterman, G., Sachse, G., and Webster, C.: Validation of Aura Microwave Limb Sounder O_3 and CO observations in the upper troposphere and lower stratosphere, J. Geophys. Res, 113, D15S02, https://doi.org/10.1029/2007JD008805, 2008.

Livesey, N. J., Read, W. G., Wagner, P. A., Froidevaux, L., Lambert, A., Manney, G. L., Valle, L. M., Pumphrey, H. C., Santee, M. L., Schwartz, M. J., Wang, S., Fuller, R. A., Jarnot, R. F., Knosp, B. W., Martinez, E., and Lay, R. R.: Earth Observing System (EOS) Aura Microwave Limb Sounder (MLS) Version 4.2x Level 2 data quality and description document., Tech. Rep. JPL D-33509 Rev D, NASA Jet Propulsion Laboratory California Institute of Technology, Pasadena, California, 91109-8099, http://mls.jpl.nasa.gov, 2018.

https://doi.org/10.5194/acp-2020-840
Preprint. Discussion started: 31 August 2020

Atmospheric Chemistry and Physics Discussions

National Centers for Environmental Prediction: NCEP FNL Operational Model Global Tropospheric Analyses, continuing from July 1999, https://doi.org/10.5065/D6M043C6, 2000.

Peterson, D. A., Campbell, J. R., Hyer, E. J., Fromm, M. D., Kablick III, G. P., Cossuth, J. H., and DeLand, M. T.: Wildfire-driven thunderstorms cause a volcano-like stratospheric injection of smoke, Nature Partner Journal: Climate and Atmospheric Science, 1, 30, https://doi.org/10.1038/s41612-018-0039-3, 2018.

Pumphrey, H. C., Filipiak, M. J., Livesey, N. J., Schwartz, M. J., Boone, C., Walker, K. A., Bernath, P., Ricaud, P., Barret, B., Clerbaux, C., Jarnot, R. F., Kovalenko, L. J., Manney, G. L., and Waters, J. W.: Validation of middle-atmosphere carbon monoxide retrievals from MLS on Aura, Journal of Geophysical Research, 112, D24S38, https://doi.org/10.1029/2007JD008723, 2007.

Pumphrey, H. C., Santee, M. L., Livesey, N. J., Schwartz, M. J., and Read, W. G.: Microwave Limb Sounder observations of biomass-burning products from the Australian bush fires of February 2009, Atmos. Chem. Phys., 11, 6285–6296, https://doi.org/10.5194/acp-11-6285-2011, http://www.atmos-chem-phys.net/11/6285/2011/, 2011.

Pumphrey, H. C., Glatthor, N., Bernath, P. F., Boone, C. D., Hannigan, J., Ortega, I., Livesey, N. J., and Read, W. G.: MLS measurements of stratospheric hydrogen cyanide during the 2015–16 El Niño event, Atmospheric Chemistry and Physics, 2018, 691–703, https://doi.org/10.5194/acp-18-691-2018, 2018.

R Core Team: R: A Language and Environment for Statistical Computing, R Foundation for Statistical Computing, Vienna, Austria, https://www.R-project.org/, 2018.

Randerson, J. T., van der Werf, G. R., Giglio, L., Collatz, G. J., and Kasibhatla, P. S.: Global Fire Emissions Database, Version 4.1 (GFEDv4), https://doi.org/10.3334/ORNLDAAC/1293, https://doi.org/10.3334/ORNLDAAC/1293, last access 15 January 2018, 2017.

Reisner, J., D'Angelo, G., Koo, E., Even, W., Hecht, M., Hunke, E., Comeau, D., Bos, R., and Cooley, J.: Climate Impact of a Regional Nuclear Weapons Exchange: An Improved Assessment Based On Detailed Source Calculations, J. Geophys. Res. Atmospheres, 123, 2752–2772, https://doi.org/10.1002/2017JD027331, 2018.

Rinsland, C. P., Dufour, G., Boone, C. D., Bernath, P. F., Chiou, L., Pierre-Fran c. C., Turquety, S., and Clerbaux, C.: Satellite boreal measurements over Alaska and Canada during June–July 2004: Simultaneous measurements of upper tropospheric CO, C_2H_6, HCN, CH_3Cl, CH_4, C_2H_2, CH_3OH, HCOOH, OCS, and SF_6 mixing ratios, Global Biogeochemical Cycles, 21, GB3008, https://doi.org/10.1029/2006GB002795, 2007.

Robock, A., Oman, L., Stenchikov, G. L., Toon, O. B., Bardeen, C., and Turco, R. P.: Climatic consequences of regional nuclear conflicts, Atmospheric Chemistry and Physics, 7, 2003–2012, https://doi.org/10.5194/acp-7-2003-2007, https://www.atmos-chem-phys.net/7/2003/2007/, 2007.

Santee, M., Livesey, N., Manney, G., Lambert, A., and Read, W.: Methyl chloride from the Aura Microwave Limb Sounder: First global climatology and assessment of variability in the upper troposphere and stratosphere, J. Geophys. Res. Atmospheres, 118, 13 532 – 13 560, https://doi.org/10.1002/2013JD020235, 2013.

Simpson, I. J., Akagi, S. K., Barletta, B., Blake, N. J., Choi, Y., Diskin, G. S., Fried, A., Fuelberg, H. E., Meinardi, S., Rowland, F. S., Vay, S. A., Weinheimer, A. J., Wennberg, P. O., Wiebring, P., Wisthaler, A., Yang, M., Yokelson, R. J., and Blake, D. R.: Boreal forest fire emissions in fresh Canadian smoke plumes: C_1-C_{10} volatile organic compounds (VOCs), CO_2, CO, NO_2, NO, HCN and CH_3CN, Atmospheric Chemistry and Physics, 11, 6445–6463, https://doi.org/10.5194/acp-11-6445-2011, https://www.atmos-chem-phys.net/11/6445/2011/, 2011.

Stohl, A., Wotawa, G., Siebert, G., and Kromp-Kolb, H.: Interpolation errors in wind fields as a function of spatial and temporal resolution and their impact on different types of kinematic trajectories, J. Appl. Meteor., 34, 2149–2165, 1995.

https://doi.org/10.5194/acp-2020-840
Preprint. Discussion started: 31 August 2020

Stohl, A., Forster, C., Frank, A., Seibert, P., and Wotawa, G.: Technical note: The Lagrangian particle dispersion model FLEXPART version 6.2, Atmos. Chem. Phys., 5, 2461–2474, 2005.

van Ravenzwaaij, D., Cassey, P., and Brown, S. D.: A simple introduction to Markov Chain Monte–Carlo sampling, Psychon. Bull. Rev., 25, 143–154, https://doi.org/10.3758/s13423-016-1015-8, 2018.

Waters, J. W., Froidevaux, L., Harwood, R., Jarnot, R., Pickett, H., Read, W., Siegel, P., Cofield, R., Filipiak, M., Flower, D., Holden, J., Lau, G., Livesey, N., Manney, G., Pumphrey, H., Santee, M., Wu, D., Cuddy, D., Lay, R., Loo, M., Perun, V., Schwartz, M., Stek, P., Thurstans, R., Boyles, M., Chandra, S., Chavez, M., Chen, G.-S., Chudasama, B., Dodge, R., Fuller, R., Girard, M., Jiang, J., Jiang, Y., Knosp, B., LaBelle, R., Lam, J., Lee, K., Miller, D., Oswald, J., Patel, N., Pukala, D., Quintero, O., Scaff, D., Snyder, W., Tope, M., Wagner, P., and Walch, M.: The Earth Observing System Microwave Limb Sounder (EOS MLS) on the Aura satellite, IEEE Trans. Geoscience and Remote Sensing, 44, 1106–1121, 2006.

Winker, D. M., Vaughan, M. A., Omar, A., Hu, Y., Powell, K. A., Liu, Z., Hunt, W. H., and Young, S. A.: Overview of the CALIPSO Mission and CALIOP Data Processing Algorithms, Journal of Atmospheric and Oceanic Technology, 26, 2310–2323, https://doi.org/10.1175/2009JTECHA1281.1, https://doi.org/10.1175/2009JTECHA1281.1, 2009.

Yu, P., Toon, O. B., Bardeen, C. G., Zhu, Y., Rosenlof, K. H., Portmann, R. W., Thornberry, T. D., Gao, R.-S., Davis, S. M., Wolf, E. T., de Gouw, J., Peterson, D. A., Fromm, M. D., and Robock, A.: Black carbon lofts wildfire smoke high into the stratosphere to form a persistent plume, Science, 365, 587–590, https://doi.org/10.1126/science.aax1748, 2019.

Zuev, V. V., Gerasimov, V. V., Nevzorov, A. V., and Savelieva, E. S.: Lidar observations of pyrocumulonimbus smoke plumes in the UTLS over Tomsk (Western Siberia, Russia) from 2000 to 2017, Atmospheric Chemistry and Physics, 19, 3341–3356, https://doi.org/10.5194/acp-19-3341-2019, https://www.atmos-chem-phys.net/19/3341/2019/, 2019.